NON-DEMOLITION DISPERSIVE MEASUREMENT OF A SUPERCONDUCTING QUBIT WITH A MICROSTRIP SQUID AMPLIFIER

G.P. BERMAN   D.I. KAMENEV

Theoretical Division and CNLS, Los Alamos National Laboratory
Los Alamos, NM 87545, USA

D. KINION

Lawrence Livermore National Laboratory
Livermore, CA 94551, USA

V.I. TSIFRINOVICH

Department of Applied Physics, Polytechnic Institute of NYU
6 MotroTech Center, Brooklyn, NY 11201, USA

We have studied the possibility of a single-shot non-demolition measurement of a superconducting qubit using a microstrip SQUID amplifier (MSA). The Johnson noise generated by all resistors in the MSA is taken into consideration. We show that a single-shot non-demolition measurement is possible with six photons in the measurement resonator.

1   Introduction

A superconducting circuit containing Josephson junctions (JJ) has attracted enormous attention of researchers developing quantum computers [1-6]. This circuit can be considered as an artificial micrometer-size atom, which can be easily integrated into sophisticated electronic architectures. One of the main problems for any implementation of quantum computing is achieving a high fidelity measurement of the qubit computational states. To do this one needs a non-demolition quantum

measurement [7]. A non-demolition measurement does not disturb the computational state. It allows one to integrate the signal and increase the signal-to-noise ratio (SNR) to that required for a high fidelity measurement.

Various schemes for non-demolition measurements of a superconducting qubit have been discussed in literature [8,9], but the only scheme implemented experimentally is the dispersive measurement designed in ref. [10]. In this method a qubit loop (QL) is coupled to a measurement resonator (MR) with a small number of photons. Due to the small number of photons and relatively large detuning between the MR and the QL, the computational quantum state of the QL remains undisturbed while the frequency of the MR becomes dependent on the qubit state. Experimental implementation of this scheme requires amplification of the MR signal. The inevitable noise generated by an amplifier became the main obstacle for a single-shot non-demolition measurement [7].

To reduce the amplifier-generated noise one could use a low-noise microstrip SQUID amplifier (MSA) [11]. At frequencies below $1\ \mathrm{GHz}$ MSAs have demonstrated a $25\ \mathrm{dB}$ power gain with an almost quantum limited noise temperature of $2hf/k_B$ [12]. However, for a dispersive measurement one has to use an MSA in the GHz frequency region. This requires reduction of the size of the MSA input coil, which diminishes its coupling with the SQUID [11]. One could raise the input voltage of the MSA increasing the number of photons in MR but this causes a back reaction of the MR on the QL, and the dispersive measurement becomes a demolition measurement [13-15].

In our work we try to find a delicate balance between the reasonable MSA parameters and the number of photons in the MR. Applying the simple model of an MSA suggested in [16] and experimental data from the non-demolition dispersive measurement with a transmon qubit [17], we show that a single-shot non-demolition dispersive measurement is possible with six photons in the MR. We believe that our estimation can also be used for a phase qubit which occupies a special place in the superconducting qubit zoo: it is especially adjusted for integration into the complicated quantum computer architecture [18].

2   Dispersive measurement of a superconducting qubit with an MSA

We consider a measurement scheme similar to that used in [17], but containing an MSA. (See Fig. 1.) A driving electromagnetic field (measurement tone) of frequency, f_m, is applied to the MR, which is coupled to the QL. The shifted frequency of the MR, f_r', equals the driving frequency, f_m, when the qubit is in its excited state, $|1\rangle$. If the qubit is in its ground state, $|0\rangle$, then $f_r' \neq f_m$. The output MR voltage is amplified by the MSA, which is tuned to the driving frequency, f_m. It is clear that the output MR voltage, which is equal to the MSA input voltage, depends on the qubit state: for the qubit excited state it is expected to be much greater than for the qubit ground state.

After amplification, the output MSA voltage is mixed with the reference signal whose frequency is slightly different from the driving frequency, f_m, (heterodyne detection). The mixed signal whose frequency is much lower than the driving frequency is finally detected. Depending on the phase of the reference signal, the amplitude of the mixed signal can represent either in-phase or the quadrature signal.
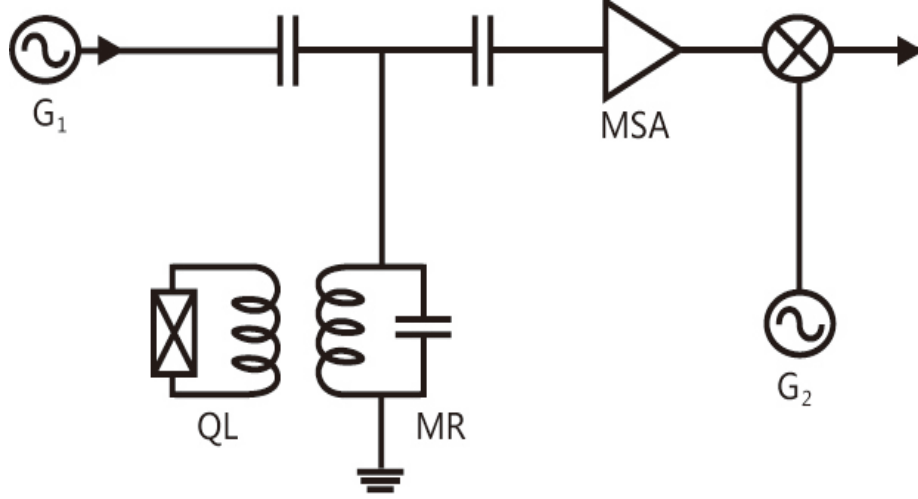
Fig. 1. Schematic of a dispersive measurement with an MSA and a heterodyne detection. G_1 is the generator of the driving electromagnetic field, G_2 is the generator of the reference signal (local generator), $\otimes$ indicates the mixer.

The non-demolition measurement of the qubit state is described by the Cavity-Bloch equations in the rotating frame [17]:

$$d_t \langle a \rangle = -i\Delta_{rm}\langle a \rangle - i\chi\langle a\sigma^z \rangle - i\varepsilon_m - (\kappa/2)\langle a \rangle,$$

$$d_t \langle \sigma^z \rangle = -\gamma_1\left(1 + \langle \sigma^z \rangle\right), \tag{1}$$

$$d_t \langle a\sigma^z \rangle = -i\Delta_{rm}\langle a\sigma^z \rangle - i\chi\langle a \rangle - i\varepsilon_m\langle \sigma^z \rangle - \gamma_1\langle a \rangle - \left(\gamma_1 + \kappa/2\right)\langle a\sigma^z \rangle.$$

Here a is the annihilation operator which describes the electromagnetic field in the MR; $\Delta_{rm} = \omega_r - \omega_m$, is the difference between the unperturbed MR frequency and the driving frequency, $\omega_k = 2\pi f_k$ for any index "k"; χ is the MR frequency shift; σ^z is the Pauli operator describing the qubit state; ε_m is the amplitude of the driving field in frequency units; κ is the MR decay constant, which is connected to the MR quality factor, Q, by the relation: $\kappa = \omega_r/Q$; and γ_1 is the decay constant for the QL, which is a reciprocal of the qubit relaxation time: $\gamma_1 = 1/T_1$. In these

equations $\langle\sigma^z\rangle=1$ for the excited qubit state. Below we put $\Delta_{rm}=-\chi$. The average number of photons in the resonator, $\langle n\rangle=\langle a^\dagger a\rangle$, is given by the equation:

$$d_t\langle n\rangle=-2\varepsilon_m\,\mathrm{Im}\langle a\rangle-\kappa\langle n\rangle\,. \tag{2}$$

The value, $\varepsilon_m=\kappa/2,$ corresponds to one photon in the MR in the stationary resonance regime with no qubit relaxation $\left(\langle\sigma^z\rangle=1,\ d_t\langle a\rangle=d_t\langle a\sigma^z\rangle=\gamma_1=0\right)$. We will consider a rectangular driving pulse: $\varepsilon_m=0$ for $t<0$, and $\varepsilon_m=\kappa/2$ for $0<t<\tau$. With initial conditions:

$$\langle\sigma^z\rangle=\pm1,\quad \langle a\rangle=0,\quad \langle a\sigma^z\rangle=0, \tag{3}$$

the Cavity-Bloch equations can be easily solved analytically. In particular, the stationary solutions with no qubit relaxation are given by the simple equations,

$$\begin{aligned}\langle a\rangle&=-2i\varepsilon_m/\kappa \text{ for } \langle\sigma^z\rangle=1,\\ \langle a\rangle&=-2i\varepsilon_m/\left(\kappa-4i\chi\right) \text{ for } \langle\sigma^z\rangle=-1.\end{aligned} \tag{4}$$

Note that for $\langle\sigma^z\rangle=1$ the stationary solution is imaginary, i.e. at the output of the MR we have only the quadrature voltage, V, which is proportional to $\mathrm{Im}\langle a\rangle$:

$$V=\left(hf_r\kappa Z\right)^{1/2}\mathrm{Im}\langle a\rangle. \tag{5}$$

Here Z is the characteristic impedance of the transmission line. Below we consider only the quadrature signals.

In Figs 2 and 3 we show the negative of the non-stationary quadrature voltage $\left(-V\right)$ for parameters that are close to the experimental parameters in [17]:

$$f_r=6.19 \text{ GHz},\ \kappa/2\pi=1.7 \text{ MHz},\ \chi/2\pi=0.7 \text{ MHz}.$$

Next, we consider amplification of the quadrature signal with the MSA. In the MSA an input coil has one end open, so the parasitic capacitances become active components of the input circuit. As a result, the theoretical description of the input circuit is not straightforward, and the suitable equivalent circuit for the MSA is unknown. Various theoretical approaches to describe the MSA have been suggested in the literature. (See, for example, [16, 19-23].) We will use here a semi-empirical model [16], which provides a reliable estimate for the MSA gain. In this model, one considers a relatively simple MSA scheme consisting of the input circuit and the SQUID. (See Fig. 4.) The trick is

that the effective parameters of the scheme are to be found from experiment assuming that the back reaction of the SQUID on the input circuit can be ignored.
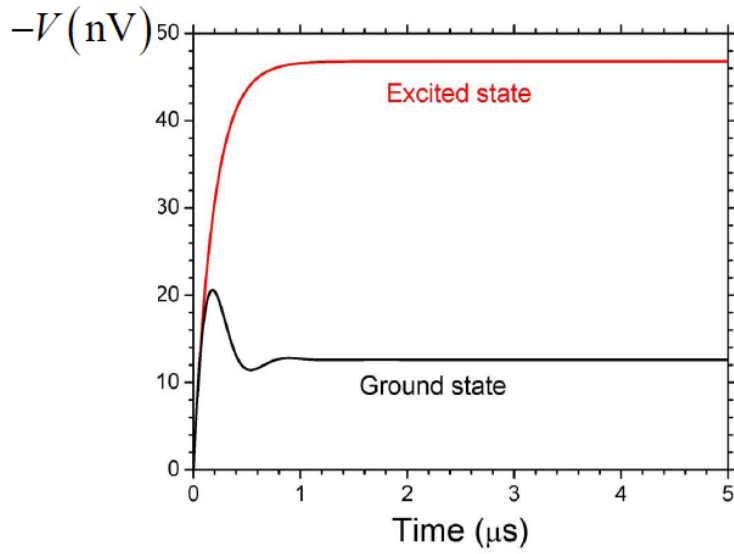
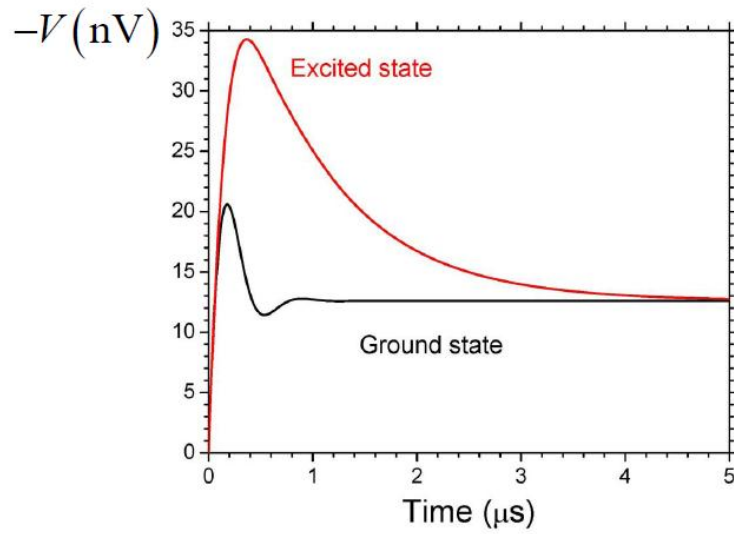Fig. 2. The negative of the quadrature voltage $(-V)$ at the output of MR for $T_1 = \infty$.

Fig. 3. The same as in Fig. 2 for $T_1 = 900$ ns.

With a harmonic input voltage, $V_{in}(t) = V\exp(i\omega t)$, the current in the input coil is given by $I_i(t) = I_i \exp(i\omega t)$. The complex amplitude of the current, I_i, can be expressed in terms of the impedances: $I_i = VZ_{LCR} / Z_L Z$, where

$$Z = R_1 + Z_{C1} + Z_{LCR},$$
$$Z_{LCR} = (Z_L^{-1} + Z_C^{-1} + R^{-1})^{-1}.$$

(6)

The time-dependent input flux from the coil to the SQUID is $MI_i(t)$. For a dispersive measurement, the MSA input frequency equals the MR driving frequency: $\omega = \omega_m$.
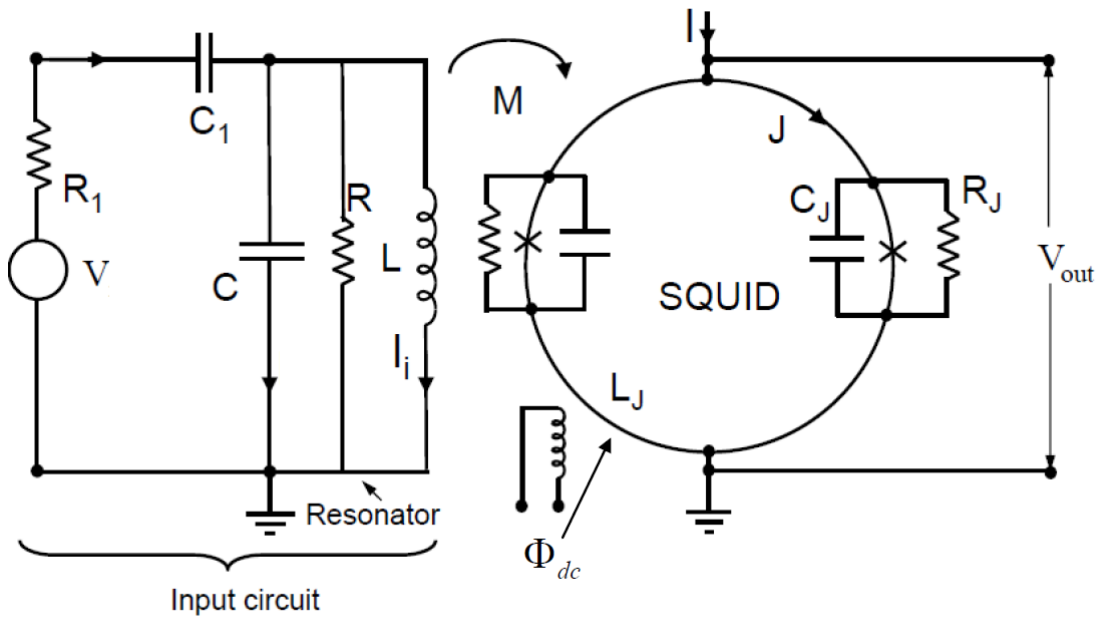

Fig. 4. The MSA equivalent circuit.

In order to compute the output MSA voltage, $V_{out}(t)$, we have solved numerically the standard system of equations for a dc SQUID [24]:

$$\varphi_0 C_J \ddot{\delta}_1 + \frac{\varphi_0}{R_J} \dot{\delta}_1 = \frac{I}{2} - J - I_0 \sin \delta_1,$$

$$\varphi_0 C_J \ddot{\delta}_2 + \frac{\varphi_0}{R_J} \dot{\delta}_2 = \frac{I}{2} + J - I_0 \sin \delta_2,$$

$$\varphi_0 (\delta_1 - \delta_2) = \Phi_{dc} + L_J J + M I_i,$$

$$V_{out}(t) = \frac{\varphi_0}{2} \left(\dot{\delta}_1 + \dot{\delta}_2 \right).$$

$$(7)$$

Here the dot above δ_1 and δ_2 indicates time differentiation; $\varphi_0 = \hbar / 2e$ is the reduced flux quantum; δ_1 and δ_2 are the phase differences across JJ; I_0 is the JJ critical current; I is the bias current; J is the circulating current; and Φ_{dc} is the dc bias flux.

Solving Eqs. (7), we compute the output MSA voltage, $V_{out}(t)$, and then find its Fourier component at the input frequency, ω. Below we use the symbol, V_{out}, for the Fourier component of the output MSA voltage. (The ratio, V_{out}/MI_i, represents the dynamical transfer function of the SQUID.) In Fig. 5 we show the power gain $G = \left| V_{out} / V \right|^2$ (in dB) as a function of the input frequency, $f = \omega/2\pi$, for the following values of parameters:

$$R_1 = 50 \ \Omega, \ C_1 = 0.12 \ \text{pF}, \ L = 0.69 \ \text{nH},$$
$$C = 0.85 \ \text{pF}, \ R = 1 \ \text{k}\Omega, \ M = 0.22 \ \text{nH}, \tag{8}$$
$$I_0 = 8 \ \mu\text{A}, \ R_J = 20 \ \Omega, \ L_J = 0.129 \ \text{nH}, \ C_J = 52.7 \ \text{fF}.$$
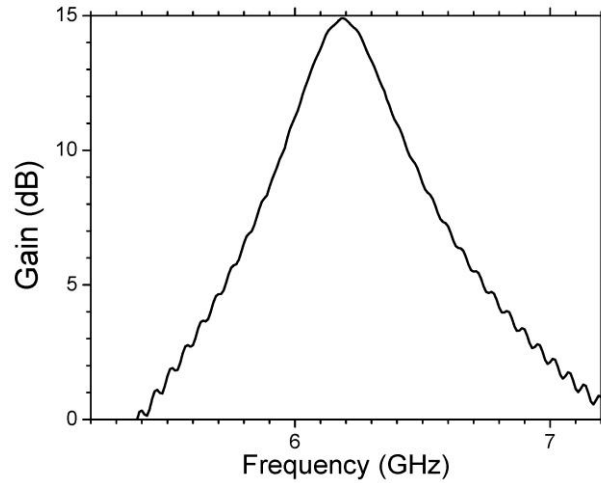

Fig. 5. The MSA power gain, $10 \log G$.

For the chosen parameters, the maximum power gain, which we denote as G_{MSA}, occurs at the frequency, $f = f_{MSA} = 6.19 \text{ GHz}$. The value of the maximum gain is 14.9 dB. The MSA bandwidth, $B_{MSA} = 340 \text{ MHz}$ (from 6.02 to 6.36 MHz, where gain decreases by 3 dB).

Next, we have computed the power spectral density of the MSA noise at the temperature, $T = 15 \text{ mK,}$ taking into consideration the Johnson noise generated by all the resistors in Fig. 4. In the input circuit in Fig. 4 we set $V_{in} = 0,$ and added the two independent sources of voltage noise in series with the resistors, R_1 and R. In the SQUID circuit in Fig. 4 we have added the two independent sources of current noise in parallel to the resistors, R_J. (The voltage noise source in series is equivalent to the current noise source in parallel.) For every realization of the Johnson noise we have solved the system of equations for the input circuit and SQUID and found the corresponding realization of the output noise voltage, $V_{out}^n(t)$. The voltage noise produced by a resistor with resistance, R_k, was approximated as white noise with the power spectral density (see, for example, [25]):

$$S_V = 2R_k h f_{MSA} \coth\left(\frac{h f_{MSA}}{2k_B T}\right). \tag{9}$$

The corresponding power spectral density for the current noise is, S_V / R_k^2. In order to simulate the white noise we have used a standard continuous chain of the short rectangular pulses with the random amplitude and zero average value. (See, for example, [24].) The power spectral density of the MSA noise at the input frequency, f, was computed using the expressions:

$$S_V(f) = \lim_{t_i \to \infty} \frac{2}{t_i}\left\langle \left|V(f)\right|^2 \right\rangle, \quad V(f) = \int_0^{t_i} V_{out}^n(t)\exp(2\pi i f t)dt. \tag{10}$$

The spectral density was computed, averaging over 300 realizations of $V_{out}^n(t)$. The maximum of the spectral density, $S_V(f)$, which we denote as S_{MSA}, was found at the same frequency, $f = f_{MSA}$, as the maximum of the gain. For our parameters we have obtained the value: $S_{MSA} = 5 \times 10^{-20} \text{ V}^2/\text{Hz}$. The MSA noise temperature, T_n, was found from equation [26]:

$$2R_1 hf_{MSA} \coth\left(\frac{hf_{MSA}}{2k_B(T_n+T)}\right)G(f_{MSA}) = S_{MSA}. \tag{11}$$

We have obtained the value, $T_n \approx 440 \text{ mK} \approx 1.5 hf_{MSA}/k_B$. Assuming that after amplification the measured signal is passing through a filter with bandwidth, $B = 2 \text{ MHz}$, we obtain the voltage noise power, $S_{MSA}B = 10^{-13} \text{ V}^2$.

Next, we estimate the SNR for a single-shot dispersive measurement with the MSA. Fig. 6 shows the difference, D, between the MSA output voltages, V_{out}, corresponding to the two qubit states for $T_1 = 900 \text{ ns}$. The values of V_{out} were obtained from the voltages shown in Fig. 3 using the computed MSA gain, G_{MSA}. The function, $D(t)$, has the maximum value, $D_{max} = 120 \text{ nV}$, at time $t = 0.46 \text{ μs}$. The maximum value of the SNR can be estimated as,

$$SNR = \frac{D_{max}}{\sqrt{S_{MSA}B}} = 0.425. \tag{12}$$
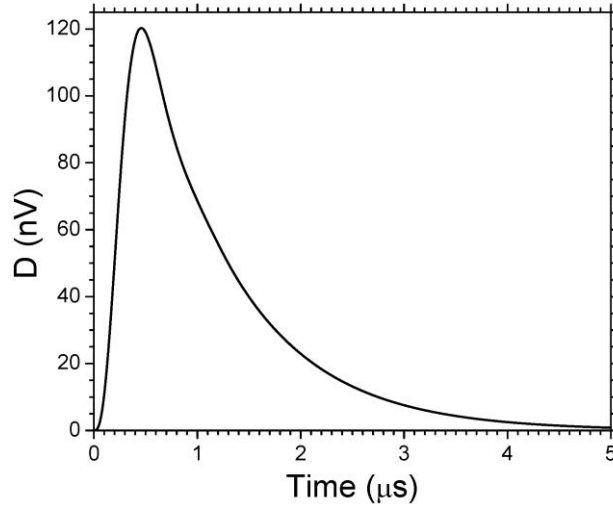

Fig. 6. The difference between the voltages corresponding to the two qubit states.

The MSA gain can be raised by increasing the resistance, R_J, in the MSA SQUID. However, our simulations show that the MSA noise grows faster than the gain, so the SNR drops. In order to obtain

$SNR > 1$, we have to increase the input voltage in the MSA by a factor of $K > 2.35$. This means that the average number of photons in the resonator must be $\langle n \rangle = K^2 > 5.5$. Our computations show that the corresponding maximum input voltage in the MSA (about 108 nV) remains in the linear range of the MSA, which extends to about $30\mu V$.

3   Conclusion

In this work we studied the possibility of a single-shot non-demolition measurement of a superconducting qubit using an MSA. We have shown that, for reasonable values of parameters, this measurement is possible with about six photons in the MR. Our results can be useful for experimental implementation of a single-shot non-demolition measurement of the superconducting qubit using an MSA. Note, that a single-shot non-demolition dispersive measurement of the transmon qubit has been recently implemented using a low-noise parametric amplifier [27].

References

1. M.H. Devoret and J.M. Martinis. Implementing qubits with superconducting integrating circuits. Quantum Information Processing, **3**, 163 (2004).

2. J.Q. You and F. Nori. Superconducting circuits and quantum information. Phys. Today, **58**, 42 (2005).

3. J. Majer, J.M. Chow, J.M. Gambetta, J. Koch, B.R.Johnson, J.A. Schreier, L. Frunzio, D.I. Schuster, A.A. Houck, A. Wallraff, A. Blais, M.H. Devoret, S.M. Girvin, and R.J. Schoelkopf. Coupling superconducting qubits via a cavity bus. Nature, **449**, 443 (2007).

4. J. Clarke and F.K. Wilhelm. Superconducting quantum bits. Nature, **453**, 1031 (2008).

5. L. DiCarlo, J.M. Chow, J.M. Gambetta, L.S. Bishop, B.R. Johnson, D.I. Schuster, J. Majer, A. Blais, L. Frunzio, S.M. Girvin, and R.J. Schoelkopf. Demonstration of two-qubit algorithms with a superconducting quantum processor. Nature, **460**, 240 (2009).

6. M. Neeley, R.C. Bialczak, M. Lenander, E. Lucero, M. Mariantoni, A.D. O'Connell, D. Sank, H. Wang, M. Weides, J. Wenner, Y. Yin, T. Yamamoto, A.N. Cleland, and J.M. Martinis. Generation of three-qubit entangled states using superconducting phase qubits. Nature, **467,** 570 (2010).

7. J. Gambetta, W.A. Braff, A. Wallraff, S.M. Girvin, and R.J. Schoelkopf. Protocols for optimal readout of qubits using a continuous quantum nondemolition measurement. Phys. Rev. A, **76,** 012325 (2007).

8. G.P. Berman, A.R. Bishop, A.A. Chumak, D. Kinion, and V.I. Tsifrinovich. Measurement of the Josephson Junction Phase Qubits by a Microstrip Resonator. arXiv:quant-ph/09123791 (2009).

9. G.P. Berman, A.A. Chumak, D.I. Kamenev, D. Kinion, and V.I. Tsifrinovich. Non-demolition adiabatic measurement of the phase qubit state. Quantum Information & Computation, **11**, 1045 (2011).

10. A. Blais, R.S. Huang, A. Wallraff, S.M. Girvin, and R.J. Schoelkopf. Cavity quantum electrodynamics for superconducting electrical circuits: An architecture for quantum computation. Phys. Rev. A, **69,** 062320 (2004).

11. M. Mück and R. McDermott. Radio-frequency amplifiers based on dc SQUIDs. Superconductor Science and Technology, **23**, 093001 (2010).

12. M. Mück, J.B. Kucia, and J. Clarke. Superconducting quantum interference device as a near-quantum- limited amplifier at 0.5 GHz. Appl. Phys. Lett., **78,** 967 (2001).

13. M. Boissonneault, J.M. Gambetta, and A. Blais. Nonlinear dispersive regime of cavity QED: The dressed dephasing model. Phys. Rev. A, **77**, 060305(R) (2008).

14. G.P. Berman and A.A. Chumak. Influence of external fields and environment on the dynamics of a phase-qubit–resonator system. Phys. Rev. A, **83**, 042322 (2011).

15. G.P. Berman, A.A. Chumak, and V.I. Tsifrinovich. Transitional dynamics of a phase qubit-resonator system: requirements for fast readout of a phase qubit. arXiv:quant-ph/1110.5566v1 (2011).

16. D. Kinion and J. Clarke. Microstrip superconducting quantum interference device radio-frequency amplifier: Scattering parameters and input coupling. Appl. Phys. Lett. **92**, 172503 (2008).

17. R. Bianchetti, S. Filipp, M. Baur, J.M. Fink, M. Göppl, P. J. Leek, L. Steffen, A. Blais, and A. Wallraff. Dynamics of dispersive single-qubit readout in circuit quantum electrodynamics. Phys. Rev. A **80**, 043840 (2009).

18. J.M. Martinis. Superconducting Phase Qubits**.** Quantum information processing, **8**, 81 (2009).

19. M. Mück and J. Clarke. The superconducting quantum interference device microstrip amplifier: Computer models. J. Appl. Phys., **88**, 6910 (2000).

20. M. Mück, J.B. Kycia, and J. Clarke. Appl. Phys. Lett., **78**, 967 (2001).

21. R. Bradley, J. Clarke, D. Kinion, L. J. Rosenberg, K. van Bibber, S. Matsuki, M. Mück, and P. Sikivie. Microwave cavity searches for dark-matter axions. Rev. Mod. Phy*s.* **75**, 777 (2003).

22. G.P. Berman, A.A. Chumak, D.I. Kamenev, D. Kinion, and V.I. Tsifrinovich. Modeling and simulation of a microstrip-SQUID amplifier. J. of Low Temp. Phys., **165**, 55 (2011).

23. G.P. Berman, A.A. Chumak, and V.I. Tsifrinovich. The renormalization effect in the microstrip SQUID amplifier. arXiv: quant-ph/ 1110.5579v1 (2011).

24. C.D. Tesche and J. Clarke. dc SQUID: Noise and optimization. J. of Low Temp. Phys., **29**, 301 (1977).

25. D. Abbott, B. R. Davis, N.J. Phillips, and K. Eshraghian. Simple derivation of the thermal noise formula using window-limited Fourier transforms and other conundrums. IEEE Transactions on Education, **39**, 1 (1996).

26. J. Clarke, A.T. Lee, M. Mück, and P. L. Richards. SQUID Voltmeters and Amplifiers. The SQUID Handbook Vol. II. Applications of SQUIDs and SQUID Systems. (Eds. J. Clarke and A.I. Braginski.) Wiley-VCH Verlag GmbH & Co. KGaA, Weinheim, p. 1-93 (2006).

27. R. Vijay, D.H. Slichter, and I. Siddiqi. Observation of quantum jumps in a superconducting artificial atom. Phys. Rev. Lett., **106**, 110502 (2011).